Sakurai, Takahiro and Saiki, Ryo and Wei, Rong Jia and Newton, Graham and Shiga, Takuya and Oshio, Hiroki (2016) Oxalate-bridged heterometallic chains with monocationic dabco derivatives. Dalton Transactions, 45 . pp. 16182-16189. ISSN 1477-9234

Journal Name

ARTICLE

Oxalate-bridged heterometallic chains with monocationic dabco derivatives

Received 00th January 20xx,
Accepted 00th January 20xx

DOI: 10.1039/x0xx00000x

www.rsc.org/

Takahiro Sakurai,[a] Ryo Saiki,[a] Rong Jia Wei,[a] Graham N. Newton,[b] Takuya Shiga [a]* and Hiroki Oshio [a]*

A series of bimetallic oxalate-bridged one-dimensional chains with monocationic dabco derivatives, ({R-dabco}[M(solv)$_2$][Cr(ox)$_3$]·n(solv) (dabco = 1,4-diazabicyclo[2.2.2]octane, H_2ox = oxalate; R = H, M = Co (**1**); R = H, M = Zn (**2**); R = Bu, M = Co (**3**); R = Bu, M = Zn (**4**)) were synthesized. All compounds have one-dimensional zig-zag chain structures with R-dabco cations located between chains. Cryomagnetic studies reveal that **1** and **3** showed intrachain ferromagnetic interactions between Co(II) and Cr(III) ions and metamagnetic behaviour due to interchain antiferromagnetic interactions. Permittivity measurements on compound **4** indicate specific paraelectronic relaxation behaviour originating from the rotational motion of the dabco alkyl substituent.

Introduction

Molecular-based functional materials can be constructed using a range of different techniques, some of which, particularly those associated with the generation of metal-organic frameworks and coordination polymers, are well developed and sophisticated.[1] Molecule-based magnets are prime examples of functional systems whose architectures are key determinants of their observable physical properties. Oxalate-bridged coordination polymers, which are well-known coordination network systems, were originally developed for their molecular magnetism, yet their potential scope of application goes beyond the borders of basic magnetism towards the field of advanced functional materials.[2]

In general, oxalate-bridged coordination polymers are constructed from the reaction of tris- or bis-(oxalato)metallate anions and free metal ions or coordinatively unsaturated complexes with appropriate counter ions. This method can be utilized towards the development of various coordination polymers with designable building units and counter ions. The dimensionality and stoichiometry of bimetallic oxalate bridged systems continue to attract research attention, and a wide variety of network structures have been constructed by trial and error.

In 1990, Ōkawa et al. reported the syntheses and magnetic properties of the hetero-metal assemblies $\{NBu_4[CuCr(ox)_3]\}_x$ and $\{[Cu(bpy)]_2[Cr(ox)_3]NO_3\}_x$; a paper that was to prove a pioneering study in molecular magnetism.[3] Ferromagnetic ordering in heterometallic oxalate networks with various combinations of metal ions was investigated.[4] Subsequently, Decurtins et al.[5] and Coronado et al.[6] reported a range of oxalate-bridged complexes with zero, one, two, and three dimensional structures. $[Cr(ox)_3]^{3-}$ and $[Fe(ox)_3]^{3-}$ ions are trianions with three coordination directions through oxalate ligands and act as connectors or 'complex ligands' in extended systems. When mixed with divalent cationic units, they can form 1:1 network structures with the supramolecular incorporation of an additional charge-balancing cation. The two dimensional honeycomb layer structure is a common motif, and several combinations of bimetallic oxalate networks and functional monocations have been reported. The chirality of complex ligands is a critical structure-directing factor, and homochiral building units can form three dimensional network structures around templating chiral cations. One dimensional network compounds of bimetallic oxalate complexes can also be constructed by the introduction of large cations and modification of the capping ligands.[7]

The physical and functional properties of oxalate-bridged systems have been widely investigated. In the early phase of research into molecular based functional materials, molecule-based magnetic materials constructed from multiple oxalate units have been studied and their magneto-structural relationships discussed. Many researchers focused on the magnetism of oxalate networks with the goal of isolating magnets with high magnetic ordering temperatures. With this historical backdrop, functional molecular materials including

[a] *Graduate School of Pure and Applied Sciences, University of Tsukuba, Tennodai 1-1-1, Tsukuba 305-8571, Japan. E-mail: oshio@chem.tsukuba.ac.jp.*
[b] *School of Chemistry, University Park Campus, University of Nottingham, Nottingham, NG7 2RD, UK*

† Footnotes relating to the title and/or authors should appear here.
Electronic Supplementary Information (ESI) available: [details of any supplementary information available should be included here]. See DOI: 10.1039/x0xx00000x

both magnetism and a second manipulable physical characteristic have emerged as a highly attractive target. Coronado et al. reported hybrid materials of BEDT-TTF and oxalate networks, which consist of Mn-Cr ferrimagnetic two-dimensionally ordered layers with conductive BEDT-TTF layers.[8] The fusion of spin-cross over components and oxalate or dithiooxalate networks with magnetic ordering have yielded examples of switchable magnets.[9] Moreover, proton-conductive oxalate networks have also been investigated,[10] as have chiral magnetic materials with unusual optical behaviour.[11] The porosity of magnets based on oxalate networks provides one potential route to the generation of multifunctional systems,[12] and such systems have been shown to exhibit a range of functionalities, including NLO activity.[13]

Magnetism and permittivity have a close relationship from the viewpoint of electromagnetism, but the construction of molecule-based compounds with synergistic interaction of magnetism and permittivity remains a very challenging theme. In the field of inorganic materials, multiferroic systems are intensively studied, as are materials that exhibit external stimuli-responsive characteristics.[14] Designer coordination compounds with electric and magnetic responses are one of the key targets for future molecule-based materials, and a wide range of systems are being studied towards this end. Herein we set out to develop functional materials with rich magnetic and dielectric properties, based on oxalate networks with 1,4-diazabicyclo[2.2.2]octane (dabco) derivatives.

Experimental

Materials and methods

All the reagents were purchased from commercial sources and used without further purification. Monocationic dabco derivatives[15], {H-dabco}BF_4 (1,4-diazabicyclo[2.2.2]octane tetrafluoroborate) and {Bu-dabco}BF_4 (1-buthyl-4-azaniabicyclo[2.2.2]octane tetrafluoroborate), were synthesized according to literature methods. $Ag_3[Cr(ox)_3]$ was prepared by metathesis from the corresponding potassium salt.[16]

Syntheses of complexes 1-4

{H-dabco}[Co(H$_2$O)$_2$][Cr(ox)$_3$]·1.5H$_2$O (1). A solution of $CoCl_2·6H_2O$ (67.4 mg, 0.283 mmol) and $Ag_3[Cr(ox)_3]$ (111 mg, 0.174 mmol) in methanol (3 mL) was stirred in the dark. The colour of the reaction mixture changed to red purple and white precipitate of AgCl was deposited. After stirring for 15 minutes, the resulting solution was filtered. To the filtrate {H-dabco}BF_4 (41.7 mg, 0.209 mmol) in water/MeOH (1:10) solution (2 mL) was added. The mixture was allowed to stand at 4°C for a few days, yielding dark red rhombic plates of {H-dabco}$[Co(H_2O)_2][Cr(ox)_3]·2CH_3OH·2H_2O$ (**1**). The crystals were collected by suction and air-dried. Yield 27.9 mg (31 %). Elemental analysis calcd. (%) for $(C_6H_{13}N_2)[Co(H_2O)_2][Cr(C_2O_4)_3]·1.5H_2O$: C 27.98, H 3.13, N 5.44; found: C 27.68, H 2.78, N 5.51. IR (KBr, cm^{-1}): 3152 (ν_{N-H}), 1634 ($\nu_{C=O}$) cm^{-1}.

{H-dabco}[Zn(H$_2$O)$_2$][Cr(ox)$_3$]·2H$_2$O (2). A similar synthetic method to that of **1**, except for the use of $ZnCl_2$ (41.4 mg, 0.304 mmol) instead of $CoCl_2·6H_2O$, to afford {H-dabco}$[Zn(H_2O)_2][Cr(ox)_3]·2CH_3OH·2H_2O$ (**2**) as purple rhombic plates. Yield 9.00 mg (11 %). Elemental analysis calcd. (%) for $(C_6H_{13}N_2)[Zn(H_2O)_2][Cr(C_2O_4)_3]·2H_2O$: C 25.43, H 3.74, N 4.94; found: C 25.53, H 3.71, N 4.99. IR (KBr, cm^{-1}): 3152 (ν_{N-H}), 1655 ($\nu_{C=O}$).

{Bu-dabco}[Co(CH$_3$OH)(H$_2$O)][Cr(ox)$_3$]·0.5H$_2$O (3). A similar synthetic method to that of **1**, except for the use of {Bu-dabco}Br (38.5 mg, 0.155 mmol) instead of {H-dabco}BF_4, to afford {Bu-dabco}$[Co(H_2O)_2][Cr(ox)_3]·2CH_3OH·2H_2O$ (**3**) as dark-red rhombic plates. Yield 33.0 mg (35 %). Elemental analysis calcd. (%) for $(C_{10}H_{21}N_2)[Co(CH_3OH)(H_2O)][Cr(C_2O_4)_3]·0.5H_2O$: C 33.84, H 4.68, N 4.64; found: C 33.88, H 4.53, N 4.59. IR (KBr, cm^{-1}): 1668 ($\nu_{C=O}$), 1626 ($\nu_{C=O}$).

{Bu-dabco}[Zn(CH$_3$OH)(H$_2$O)][Cr(ox)$_3$]·0.5H$_2$O (4). A similar synthetic method to that of **3**, except for the use of $ZnCl_2$ (41.4 mg, 0.304 mmol) instead of $CoCl_2·6H_2O$. The resulting solution was left to stand for a few days at 40 °C, affording {Bu-dabco}$[Zn(CH_3OH)(H_2O)][Cr(ox)_3]·0.5H_2O$ (**4**) as purple rhombic plates. Yield 10.0 mg (11%). Elemental analysis calcd. (%) for $(C_{10}H_{21}N_2)[Zn(CH_3OH)(H_2O)][Cr(C_2O_4)_3]·0.5H_2O$: C 33.48, H 4.63, N 4.59; found: C 33.39, H 4.38, N 4.47. IR (KBr, cm^{-1}): 1662 ($\nu_{C=O}$), 1634 ($\nu_{C=O}$).

X-ray structure determinations

Data collections were performed on a Bruker SMART APEX II for all complexes with a CCD area detector with graphite monochromated Mo-Kα (λ = 0.71073 Å) radiation. All structures were solved by direct methods and refined by full-matrix least-squares methods based on F^2 using the SHELXL software.[17] Non-hydrogen atoms were refined anisotropically. All the hydrogen atoms were positioned geometrically and refined with isotropic displacement parameters according to the riding model. All geometrical calculations were performed using the SHELXL-2014 software.

Physical measurements

Infrared (IR) spectra were recorded (400 - 4000 cm^{-1}) on a SHIMADZU FT-IR 8400 spectrometer using KBr pellets. Direct current magnetic susceptibility measurements of polycrystalline samples were measured in the temperature range of 1.8 - 300 K with a Quantum Design MPMS-5XL SQUID magnetometer under an applied magnetic field of 0.05 T. Data were corrected for the diamagnetic contribution calculated from Pascal's constants including the contribution of the sample holder. Permittivity measurements were performed using an Agilent E4980A LCR meter for pellet samples with gold wire and gold paste or powder samples with copper plate electrodes. The temperature of permittivity measurements was controlled by an Oxford mercury iTC system. Differential scanning calorimetry (DSC) measurements were performed

using an EXSTAR X-DSC7000 (Seiko Instruments Inc.) with an Al_2O_3 reference.

Results and discussion

Syntheses

Use of $Ag_3[Cr(ox)_3]$ as a starting material is known to be a clean technique for the construction of oxalate bridged network compounds.[18] During the complexation reaction, neutral self-assembled one-dimensional networks were formed in the presence of dabco derivative counter cations.

Crystal structures of 1-4

Complex **1** crystalized in monoclinic *Cc* space group, which belongs to a polar point group. The asymmetric unit includes one tris-oxalato chromium unit, a cobalt ion, two coordinated water molecules, and a H-dabco$^+$ countercation with one water and one methanol molecule in the lattice (Figures 1 and S1). The Cr ion has octahedral geometry with six oxygen donor atoms from the oxalate ligands. The Co ion has octahedral coordination geometry with four oxygen donor atoms from neighbouring $[Cr(ox)_3]^{3-}$ units and two water molecules. The average coordination bond lengths of Cr and Co ions are 1.973(1) and 2.096(1) Å, respectively. Considering charge balance and bond lengths, Co ion is assigned as divalent and high spin. The one-dimensional oxalate zig-zag chain networks consisting of $[Cr(ox)_3]^{3-}$ unit and Co^{2+} ion extend along the (1 -1 0) or (1 1 0) direction, in the *ab* plane. Two oxalate ions of the $[Cr(ox)_3]^{3-}$ units link to Co^{2+} ions in *cis* fashion, forming a zig-zag one-dimensional chain structure. The crystal-packing diagram of complex **1** (Figure 2) shows a layered structure in which each layer is composed of sheets of parallel chains along the *ab* plane. The shortest Co1-Cr1 separation through oxalate anions in the chain is 5.3826(8) Å, while the shortest gap between interchain paramagnetic centers is Co1-Co1* with a distance of 7.327(1) Å (symmetry operations *: x+1/2, y-1/2, z).

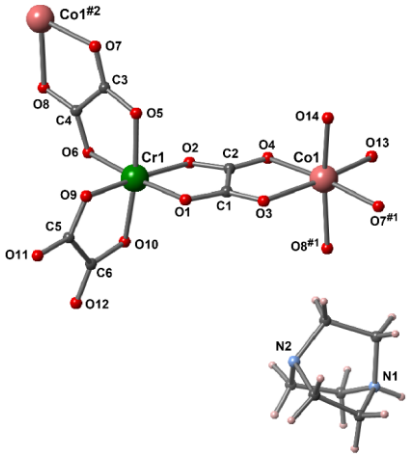

Figure 1 Asymmetric structure of **1**. Solvent molecules in the crystal lattice were omitted for clarity. Colour code: green, Cr; pink, Co; red, O; grey, C; cyan, N. Symmetry operation code: #1, +x-1/2, +y-1/2, +z; #2, +x+1/2, +y+1/2, +z.

H-dabco cations are located between the chains and interact with the non-bridging oxalate ligand (C5-C6, O9-O12) of the $[Cr(ox)_3]^{3-}$ unit through hydrogen bonding, in which $d_{N1\text{-}O11\#}$ is 2.754(4) Å and $d_{N1\text{-}O12\#}$ is 3.039(4) Å (#: x-1/2, -y+1/2, z+1/2), forming a N1-O11#-O12# triangle. The lattice is also occupied by hydrogen bonding solvent molecules.

Complex **2** has a similar one-dimensional network structure to complex **1**, however, the packing arrangement is different (Figures S2-S3). The $[Cr(ox)_3]^{3-}$ unit has the same structure as that of complex **1**, while the Zn^{2+} ion has a slightly distorted octahedral geometry with six oxygen donor atoms from two oxalate ions and two water molecules. The average coordination bond length for the Zn ion is 2.099(1) Å, a typical value for divalent Zn ions. The shortest Zn1-Cr1 separation through oxalate anions in the chain is 5.398(2) Å, while the shortest gap between interchain metal ions is Zn1-Cr1* with a distance of 7.042(2) Å (symmetry operations *: x+1/2, -y+3/2, z-1/2). The H-dabco molecule also interacts with the oxygen atoms of the oxalate moiety in the neighboring chain through hydrogen bonds, in which interatomic distances of $d_{N1\text{-}O11\#}$ and $d_{N1\text{-}O12\#}$ are 2.746(5) Å and 3.041(5) Å (#: x+1/2, -y+1/2, z-1/2), respectively.

Complex **3** also forms a one-dimensional zig-zag chain structure similar to that of **1** and **2** (Figures S4-S5). Compared to the network structures of **1** and **2**, however, complex **3** has parallel aligned crystal packing. **3** crystalized in the monoclinic $P2_1$ space group. The Cr ion has octahedral geometry with six oxygen donor atoms from oxalate ligands, and the Co ion has octahedral coordination geometry with four oxygen donor atoms from neighbouring $[Cr(ox)_3]^{3-}$ units and one water and one methanol molecule. The average coordination bond lengths around Cr and Co ions are 1.970(3) and 2.087(3) Å, respectively. Considering charge balance and bond lengths, the Co ion is assigned as divalent. One-dimensional oxalato networks consisting of $[Cr(ox)_3]^{3-}$ units and Co^{2+} ions are extended along the (1 0 0) direction. All chains are aligned along the *a* axis in the crystal lattice. The shortest Co1-Cr1 separation through oxalate anions in the chain is 5.317(2) Å. The shortest distance between interchain paramagnetic centers is Co1-Co1* with a distance of 6.831(2) Å (symmetry operations *: -x, y+1/2, -z+1).

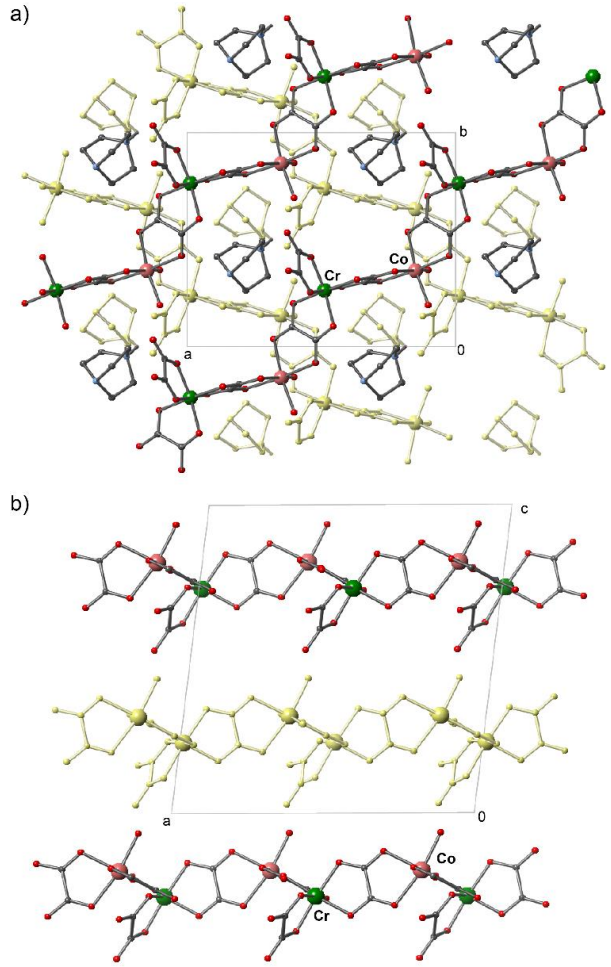

Figure 2 Packing structure of **1**. Solvent molecules were omitted for clarity. (a) *c* axis projection. (b) *b* axis projection.

Bu-dabco cations are situated between the one-dimensional chains, stabilized by hydrogen bonded interactions between the amine group of the Bu-dabco cation and a Co-coordinating water molecule, with interatomic distance of $d_{N2\text{-}O13\#}$ = 2.77(1) Å (#: -x+2, y-1/2, -z+1).

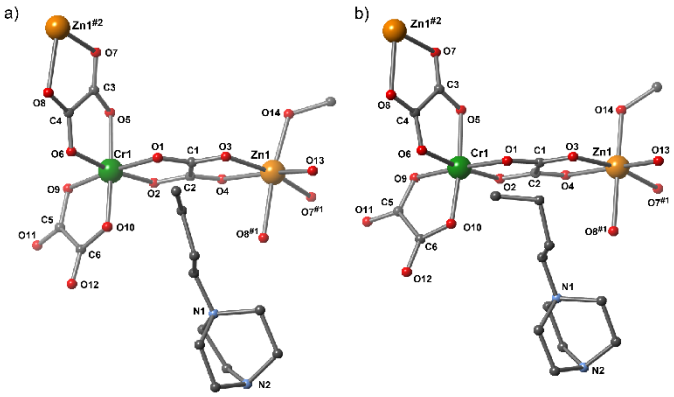

Figure 3 Asymmetric structure of **4** at (a) 100 K and (b) 130 K. Colour code: green, Cr; orange, Zn; red, O; grey, C; cyan, N. Solvent molecules were omitted for clarity. Symmetry operation code: #1, +x+1, +y, +z; #2, +x-1, +y, +z.

Complex **4** has a similar crystal structure to complex **3** (Figures 3, 4, S6, S7), and the same packing arrangement. The average coordination bond length around the Zn ion is 1.971(2) Å at 100 K, typical for divalent Zn ions. The shortest oxalate-bridged Zn1-Cr1 separation is 5.320(2) Å, while the shortest interchain gap between metal ions is Zn1-Co1* with a distance of 7.285(3) Å (symmetry operations *: -x+1, y+1/2, -z+1). At 100K, the Bu-dabco cation has *anti*-type conformation, while at 130 K it adopts a *gauche*-type arrangement. The torsion angles of C8-C9-C10-C11 at 100 K and 130 K are 173.4(6)˚ and 74.0(11)˚, respectively. This structural change is related to a specific relaxation of permittivity (*vide infra*). The coordination environments of the Zn and Cr ions showed differences between 100 K and 130 K. The distortion parameters Σ around Zn and Cr are 63.3 and 47.0 at 100 K, and 55.2 and 43.0 at 130 K, respectively.[19] This structural change of coordination geometry results from changes in the orientation of the flexible alkyl chain of Bu-dabco.

Magnetic properties of 1 and 3

Magnetic measurements for **1** and **3** were performed. It can be expected that magnetic properties for compounds **2** and **4** would show negligible magnetic interactions between Cr(III) ions through diamagnetic Zn(II) ions. Temperature dependent magnetic susceptibility for **1** was measured under a 500 Oe dc field. $\chi_m T$ versus T plots for **1** are shown in Figure 5. The $\chi_m T$ values at 300 K are larger than the spin only value 3.75 emu mol^{-1} K, which is expected from magnetically isolated Cr(III) and Co(II) ions. The deviation comes from the large magnetic anisotropy of Co(II) ions. As the temperature is lowered, the $\chi_m T$ value increased, reaching a maximum of 21.9 emu mol^{-1} K at 4 K, before decreasing to a value of 4.41 emu mol^{-1} K at 1.8 K due to saturation of magnetization or antiferromagnetic interactions between chains. Curie-Weiss plots in the temperature range of 50-300 K provide C = 4.47 emu mol^{-1} K and θ = +2.77 K. This magnetic behaviour suggests ferromagnetic interactions between intrachain Co(II) and Cr(III) ions and magnetic ordering. This corresponds to magneto-structural correlations of similar oxalate-bridged Co(II)-Cr(III) systems, and means that the magnetic behaviour of **1** can be considered as ferromagnetic chain.[20]

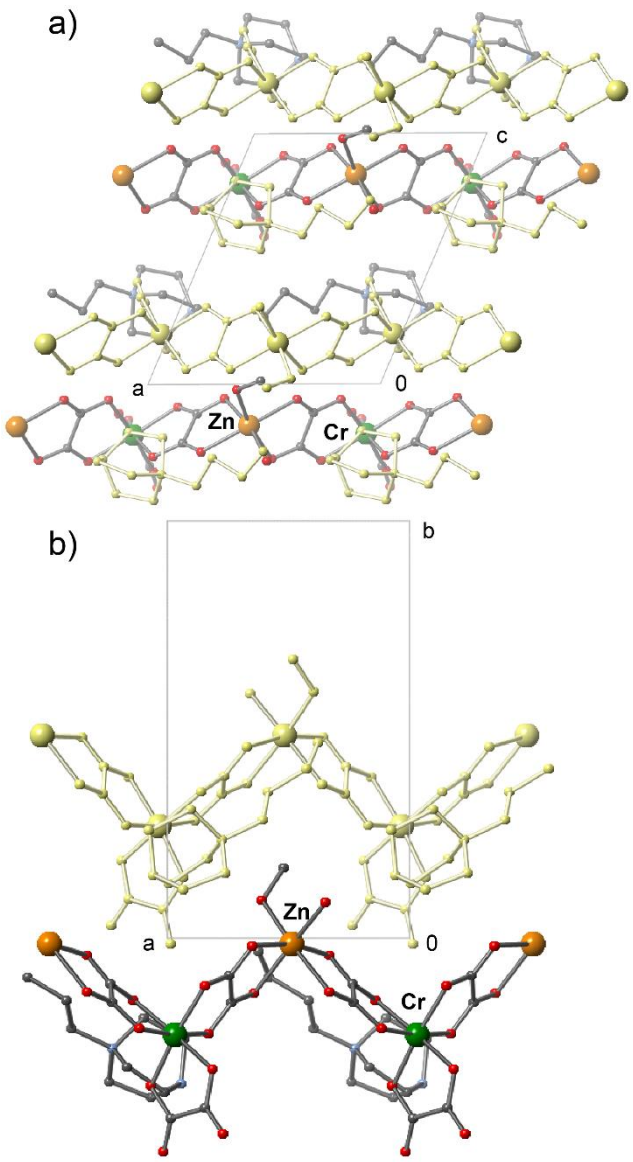

Figure 4 Packing structure of **4** at 100 K. Solvent molecules omitted for clarity.

Weak field measurements were performed and the data are shown in Figure 5 inset. Superimposition of the ZFC (zero-field cooled) curve of ZFC and the FC (field cooled) magnetization across all temperatures indicates the absence of a ferromagnetic phase. The maximum value of magnetization was observed at 4.4 K, corresponding to the Néel point. In magnetization measurements at 1.8 K a critical point relating to spin flip was observed at 840 Oe (Figure 6), clearly indicating metamagnetic behaviour. Magnetic susceptibilities under variable dc fields were investigated in order to confirm this conclusion (Figure S8). Below the magnetic ordering temperature, T_N = 4.4 K, the shape of the $\chi_m T$ vs. T curve were drastically changed around critical field.

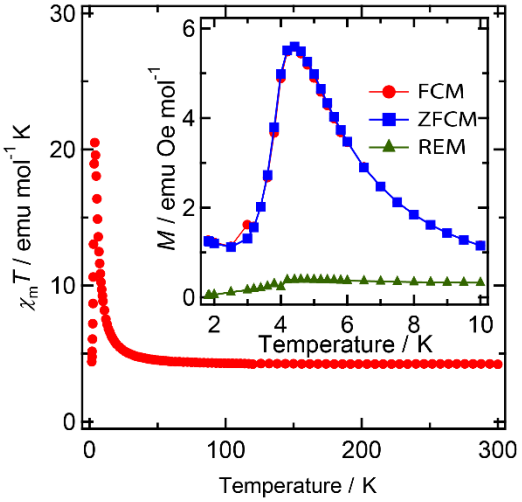

Figure 5 Temperature dependence of $\chi_m T$ for **1** under 500 Oe. Inset: Field cooled magnetization (FCM), zero-field cooled magnetization (ZFCM), and remnant magnetization (REM) under 20 Oe dc magnetic field.

The hysteresis curve for **1** at 1.8 K is shown in Figure 6. There is no remnant magnetization and no coercive field due to the meta-magnetic phase. The saturated magnetization at 5 Tesla is 0.90 emu Oe mol^{-1}, corresponding to 3.94 $N\beta$, indicative of a ferromagnetic arrangement of cobalt and chromium spins.

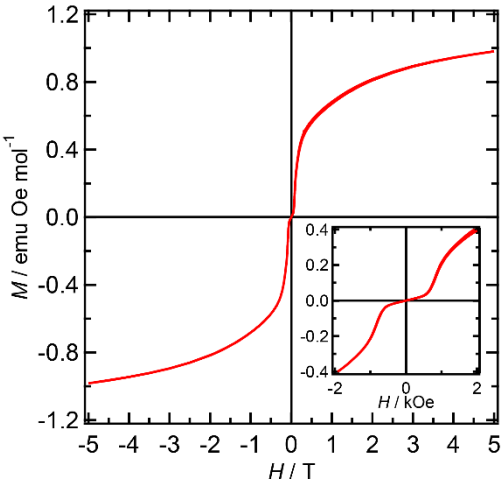

Figure 6 Magnetic hysteresis loops for **1** at 1.8 K. Inset: measurements enlarged in the low-field region.

In the case of **3**, as in **1**, intrachain ferromagnetic interactions and metamagnetic behaviour based on interchain antiferromagnetic interactions was observed. $\chi_m T$ versus T plots for **3** are shown in Figure 7. The $\chi_m T$ value at 300 K is 4.97 emu mol^{-1} K, larger than the spin only value 3.75 emu mol^{-1} K for isolated Cr(III) and Co(II) ions. This deviation again comes from the large magnetic anisotropy arising from spin-orbit coupling in Co(II) ions. As the temperature was lowered, the $\chi_m T$ value increased reaching a maximum of 30.9 emu mol^{-1} K at 4 K, before decreasing to 4.94 emu mol^{-1} K at 1.8 K due to saturation of magnetization or antiferromagnetic interactions between chains. Curie-Weiss plots in the

temperature range of 50-300 K provide C = 4.89 emu mol^{-1} K and θ = +5.65 K.

Weak field measurements were performed in order to elucidate the detailed spin structure (Figure 7 inset). The field cooled magnetization curve (FCM) shows an abrupt rise of the magnetization value below 4 K, indicating long-range magnetic ordering. The zero-field cooled magnetization curve (ZFCM) has a distinct peak at 4 K, which can be assumed to be the critical temperature of magnetic ordering. Remnant magnetization (REM) vanishes above 4 K. These magnetic properties can be observed in typical magnets.

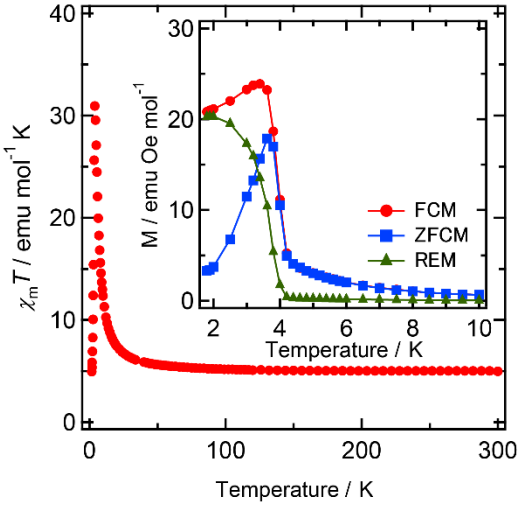

Figure 7 Temperature dependence of $\chi_m T$ for **3** under 500 Oe. Inset: Field cooled magnetization (FCM), zero-field cooled magnetization (ZFCM), and remnant magnetization (REM).

The hysteresis curve for **3** was measured at 1.8 K (Figure 8). There is inflection point at 640 Oe, which suggests metamagnetic behaviour. Remnant magnetization and coercive field were 0.008 emu Oe mol^{-1} and 140 Oe, respectively. The existence of an open hysteresis loop indicates the existence of a canted spin structure caused by interchain antiferromagnetic interactions. Considering the structural features, neighbouring paramagnetic centres between the chains are related by a 2_1 symmetry operation, an acceptable spin canting configuration.

To get further insight of the spin structures, ac magnetic susceptibilities were measured in the temperature range of 1.8 – 4.2 K (Figure S9). In the out-of-phase response, there is a peak top around 3.8 K and frequency dependence. Assuming a spin-glass phase, a value of ϕ = 0.0027 was estimated, which is close to the typical value of spin glass.[21] Arrhenius plots of the ac response allow calculation of the activation energy as E_a = 30.34 K with a pre-exponential factor of ω_0 = 6.99 x 10^{-15} Hz (Figure S10). Differences in magnetic behaviour between complexes **1** and **3** can be explained by consideration of their contrasting lattice structures. **1** has a layered structure of parallel Co-Cr chains, while **3** has aligned Co-Cr chains along the a axis. In **1**, interchain antiferromagnetic interactions between ferromagnetic Co-Cr chains were operative resulting in perfectly cancelled-out antiferromagnetic spin alignment and metamagnetic behavior. On the other hand, interchain antiferromagnetic interactions in **3** lead to spin canting due to the 2_1 screw axis, and again result in metamagnetic behaviour with canted spin moments.

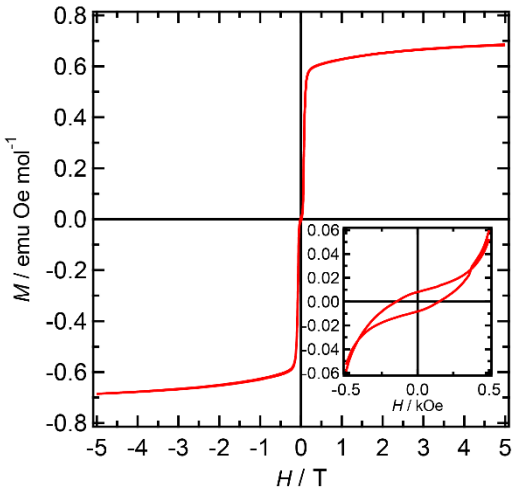

Figure 8 Magnetic hysteresis loops for **3** at 1.8 K. Inset: measurements enlarged around small fields.

Permittivity properties of 3 and 4

Dielectric permittivity measurements for **3** and **4**, which have a similar network structure incorporating Bu-dabco cations, were performed at 50 kHz - 750 kHz over the temperature range of 100 to 300 K. In **3**, gradual increases of the real and imaginary dielectric constants were observed as temperature increased (Figure S11). This behaviour is derived from contributions from the measurement environment (electrode and cell). On the other hand, complex **4** shows dielectric relaxation behaviour around 170 K - 190 K (Figure 9a). The imaginary part has a distinct peak and clear frequency dependence, indicative of thermally activated molecular motion. The peak shift was analysed by Arrhenius plots, and after least-square fitting, an activation energy of 32 kJ mol^{-1} and pre-exponential factor of 2.1 x 10^{-13} sec were obtained (Figure 9b). DFT calculations were performed to probe the rotational motion of the terminal methyl group of the Bu-dabco cation. The computation yielded an activation energy of 33.8 kJ mol^{-1} (Figure S12 and Table S1. Theoretical calculation by DFT method described in ESI), matching the experimental data and supporting our hypothesis that the methyl group acts as a molecular rotor.[22] A synthetic strategy for molecular rotors is established by supramolecular chemistry. Stators play an important role in the appearance of rotational motions, providing the stable base for the motional freedom of the rotator units. In this work, complex **3** exhibited no dielectric relaxation, but **4** showed a clear response. This difference is likely to arise from subtle differences in the crystal packing structures.

DSC measurements were performed to confirm the rotational motion. The DSC plot of **4** is shown in Figure S13. **4** showed a broad endothermic anomaly around 125 K in the heating process, and a broad exothermic peak was observed around 135 K in the cooling process. This observed temperature range is close to the region in which the dielectric response was observed. Considering the rotation motion of the terminal methyl group of butyl chain in a comprehensive way based on X-ray crystallography, permittivity, and DSC measurements, the dielectric properties of **4** can be concluded to be derived from the molecular motion of Bu-dabco.

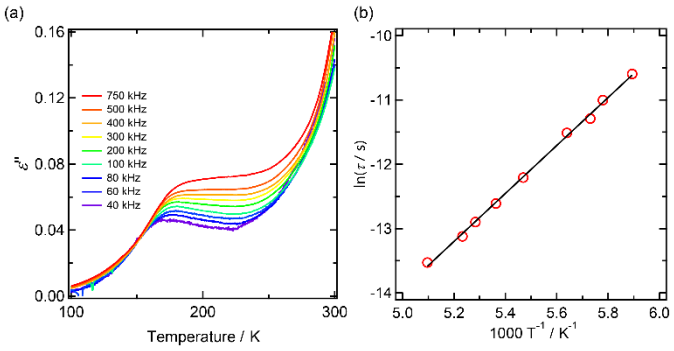

Figure 9 Dielectric properties of **4**. (a) Imaginary part of dielectric response. (b) Arrhenius plot of observed dielectric relaxation peaks.

Conclusions

Four kinds of bimetallic oxalate-bridged one-dimensional chains with monocationic dabco derivatives were synthesized by the reaction of $[Cr(ox)_3]^{3-}$ with cobalt or zinc chloride in the presence of dabco cations. Cryomagnetic studies revealed that **1** and **3** showed intrachain ferromagnetic interactions between Co(II) and Cr(III) ions and metamagnetic behaviour due to interchain antiferromagnetic interactions. This metamagnetic behaviour can be explained from the differences between the crystal packing of the chains. Permittivity measurements on **4** indicated specific paraelectronic relaxation behaviour originating from the rotational motion of a methyl group at the end of a dabco cation substituent group. These results toward the construction of magnetically-ordered and dielectric materials indicated that the combination of the traditional linkage of paramagnetic centres and the introduction of flexible cations with specific dielectric responses is a good strategy for the development of multi-functional, multi-responsive molecular materials.

Acknowledgements

This work was supported by a Grant-in-Aid for Scientific Research on (no.25248014 and no. 26410065) from the Japan Society for the Promotion of Science (JSPS).

Notes and references

‡ Structures, additional magnetic properties, permittivity data and DSC data were indicated in ESI.

1 MOF and Coordination Polymer Review: S. Kitagawa, R. Kitaura and S. Noro, *Angew. Chem., Int. Ed.*, 2004, **43**, 2334-2375; H. -C. Zhou, J. R. Long and O. M. Yaghi, *Chem. Rev.*, 2012, **112**, 673-674 (2012 Metal-Organic Frameworks Themed Issue); O. K. Farha, J. T. Hupp, *Acc. Chem. Res.*, 2010, **43**, 1166-1175; E. Coronado and G. M. Espallargas, *Chem. Soc. Rev.*, 2013, **42**, 1525-1539; C.N.R. Rao, S. Natarajan, R. Vaidhyanathan, *Angew. Chem. Int. Ed.*, 2004, **43**, 1466-1496.

2 Oxalate based magnetic materials and functional materials review: M. Clemente-León, E. Coronado, C. Martí-Gastaldo and F. M. Romero, *Chem. Soc. Rev.*, 2011, **40**, 473-497; M. Gruselle, C. Train, K. Boubekeur, P. Gredin and N. Ovanesyan, *Coord. Chem. Rev.*, 2006, **250**, 2491-2500.

3 Z. J. Zhong, N. Matsumoto, H. Okawa S. Kida, *Chem. Lett.*, 1990, 87-90.

4 H. Tamaki, Z.J. Zhong, N. Matsumoto, S. Kida, M. Koikawa, N. Achiwa, Y. Hashimoto and H. Ōkawa, *J. Am. Chem. Soc.*, 1992, **114**, 6974-6979; H. Tamaki, M. Mitsumi, K. Nakamura, N. Matsumoto, S. Kida, H. Ōkawa and S. Iijima, *Chem. Lett.*, 1992, 1975-1978; E. Pardo, C. Train, K. Boubekeur, G. Gontard, J. Cano, F. Lloret, K. Nakatani and M. Verdaguer, *Inorg. Chem.*, 2012, **51**, 11582-11593; N. Marino, D. Armentano, G.D. Munno, F. Lloret, J. Cano and M. Julve, *Dalton Trans.*, 2015, **44**, 11040-11051; P. Bhatt, N. Thakur, S.S. Meena, M.D. Mukadam and S.M. Yusuf, *J. Mater. Chem. C*, 2013, **1**, 6637-6652.

5 S. Decurtins, H. W. Schmalle, P. Schneuwly and H. R. Oswald, *Inorg. Chem.*, 1993, **32**, 1888-1892; S. Decurtins, H. W. Schmalle, H. R. Oswald, A. Linden, J. Ensling, P. Gütlich, A. Hauser, *Inorg. Chim. Acta*, 1994, **216**, 65-73; S. Decurtins, H.W. Schmalle, P. Schneuwly, J. Ensling and P. Gütlich, *J. Am. Chem. Soc.*, 1994, **116**, 9521-9528.

6 Coronado's oxalate: E. Coronado, J.R. Galán-Mascarós and C. Martí-Gastaldo, *J. Am. Chem. Soc.*, 2008, **130**, 14987-14989.

7 E. Pardo, C. Train, K. Boubekeur, G. Gontard, J. Cano, F. Lloret, K. Nakatani and M. Verdaguer, Inorg. Chem., 2012, 51, 11582-11593.

8 Coronado, BEDT-TTF Mn-Cr: E. Coronado, J.R. Galán-Mascarós, C.J. Gómez-García, V. Laukhin, *Nature*, 2000, **408**, 447-449.

9 M. Clemente-León, E. Coronado, M. López-Jordà, C. Desplanches, S. Asthana, H. Wang and J.-F. Létard, *Chem. Sci.*, 2011, **2**, 1121-1127; N. Kida, M. Hikita, I. Kashima, M. Okubo, M. Itoi, M. Enomoto, K. Kato, M. Takata and N. Kojima, *J. Am. Chem. Soc.*, 2009, **131**, 212-220.

10 Proton conduction in oxalato network: H. Ōkawa, A. Shigematsu, M. Sadakiyo, T. Miyagawa, K. Yoneda, M. Ohba and H. Kitagawa, *J. Am. Chem. Soc.*, 2009, **131**, 13516-13522; E. Pardo, C. Train, G. Gontard, K. Boubekeur, O. Fabelo, H. Liu, B. Dkhil, F. Lloret, K. Nakagawa, H. Tokoro, S.-i. Ohkoshi and M. Verdaguer, *J. Am. Chem. Soc.*, 2011, **133**, 15328-15331; M. Sadakiyo, H. Ōkawa, A. Shigematsu, M. Ohba, T. Yamada and H. Kitagawa, *J. Am. Chem. Soc.*, 2012, **134**, 5472-5475; H. Ōkawa, M. Sadakiyo, T. Yamada, M. Maesato, M. Ohba and H. Kitagawa, *J. Am. Chem. Soc.*, 2013, **135**, 2256-2262; H. Ōkawa, M. Sadakiyo, K. Otsubo, K. Yoneda, T. Yamada, M. Ohba and H. Kitagawa, *Inorg. Chem.*, 2015, **54**, 8529-8535.

11 C. Train, R. Gheorghe, V. Krstic, L.-M. Chamoreau, N.S. Ovanesyan, G.L.J.A. Rikken, M. Gruselle and M. Verdaguer, *Nat. Mat.*, 2008, **7**, 729-734.

12 Porous magnets for gas absorption: P. Dechambenoit and J.R. Long, *Chem. Soc. Rev.*, 2011, **40**, 3249-3265.

13 E. Cariati, R. Macchi, D. Roberto, R. Ugo, S. Galli, N. Casati, P. Macchi, A. Sironi, L. Bogani, A. Caneschi and D. Gatteschi, *J. Am. Chem. Soc.*, 2007, **129**, 9410-9420; C. Train, T. Nuida, R. Gheorghe, M. Gruselle and S.-i. Ohkoshi, *J. Am. Chem. Soc.*,

2009, **131**, 16838-16843; E. Coronado, C. Martí-Gastaldo, J.R. Galán-Mascarós and M. Cavallini, *J. Am. Chem. Soc.*, 2010, **132**, 5456-5468; M. Clemente-León, E. Coronado, M. López-Jordà, C. Desplanches, S. Asthana, H. Wang and J.-F Létard, *Chem. Sci.*, 2011, **2**, 1121-1127.

14 Multiferro M-E effects Inorganic materials: T. Kimura, T. Goto, H. Shintani, K. Ishizaka, T. Arima and Y. Tokura, *Nature*, 2003, **426**, 55-58; M. Mochizuki, *Phys. Rev. B*, 2015, **92**, 224412.

15 Syntheses of dabco derivatives: A. Budzianowski, A. Katrusiak and M. Szafranski, *J. Phys. Chem. B*, 2008, **112**, 16619-16625; A. Katrusiak and M. Szafrański, *Phys. Rev. Lett.*, 1999, **82**, 576-579; A. Wykes and S. L. Macneil, *Synlett*, 2007, **1**, 0107-0110; Z. -Z. Yang, L. -N. He, S. -Y. Peng and A. -H. Liu, *Green Chem.*, 2010, **12**, 1850-1854; R. Engel, J. I. Rizzo, C. Rivera, M. Ramirez, M. L. Huang, D. Montenegro, C. Copodiferro, V. Behaj, M. Thomas, B. Klaritch-vrana and J. F. Engel, *Chem. Phys. Lipids.*, 2009, **158**, 61; F. Xu, H. Chen, H. Zhang, G. Cheng and X. Zhou. *J. Mol. Struct*., 2012, **1017**, 14.

16 Synthesis of $Ag_3[Cr(ox)_3]$: J.C. Baylar, E.M. Jones, In *Inorganic Synthesis*; H.S. Booth, Ed.; McGraw-Hill: New York, 1939, **1**, 35.

17 G.M. Sheldrick, SHELXTL Version 2014/7. http://shelx.uni-ac.gwdg.de/SHELX/index.php

18 P. A. W. Dean, D. Craig, I. Dance, V. Russell and M. Scudder, *Inorg. Chem.*, 2004, **43**, 443-449; E. Coronado, J.R. Galán-Mascarós and C. Martí-Gastaldo, *Inorg. Chem.*, 2007, **46**, 8108-8110.

19 M. G. B. Drew, C. J. Harding, V. McKee, G. G. Morgan and J. Nelson, J. *Chem. Soc. Chem. Commun.*, 1995, 1035-1038.

20 Oxalate bridged Co(II)-Cr(III): M. Ohba, H. Tamaki, N. matsumoto and H. Ōkawa, *Inorg. Chem.*, 1993, **32**, 5385-5390; H.-Z. Kou and O. Sato, *Dalton Trans.*, 2008, 3652-3654; J. Vallejo, I. Castro, L. Cañadillas-Delgado, C. Ruiz-Pérez, J. Ferrando-Soria, R. Ruiz-García, J. Cano, F. Lloreta and M. Julve, *Dalton Trans.*, 2010, **39**, 2350-2358.

21 J. A. Mydosh, *Spin glasses: an experimental introduction.* Taylor & Francis Ltd., London.

22 C.S. Vogelsberg and M.A. Garcia-Garibay, *Chem. Soc. Rev.*, 2012, **41**, 1892-1910.